Meteorol. Atmos. Phys. 52, 15–35 (1993)

Meteorology and Atmospheric Physics



551.515.4:551.515.5

[1] Centre for Theoretical Studies, Indian Institute of Science, Bangalore, India
[2] Program in Atmospheric and Oceanic Sciences, University of Colorado, Boulder, Colorado, USA

# Meridional Propagation of Large-Scale Monsoon Convective Zones

**J. Srinivasan[1], S. Gadgil[1], and P. J. Webster[2]**

With 13 Figures

Received 1 May, 1992

**Summary**

Observational studies indicate that the convective activity of the monsoon systems undergo intraseasonal variations with multi-week time scales. The zone of maximum monsoon convection exhibits substantial transient behavior with successive propagating from the North Indian Ocean to the heated continent. Over South Asia the zone achieves its maximum intensity. These propagations may extend over 3000 km in latitude and perhaps twice the distance in longitude and remain as coherent entities for periods greater than 2–3 weeks. Attempts to explain this phenomena using simple ocean-atmosphere models of the monsoon system had concluded that the interactive ground hydrology so modifies the total heating of the atmosphere that a steady state solution is not possible, thus promoting lateral propagation. That is, the ground hydrology forces the total heating of the atmosphere and the vertical velocity to be slightly out of phase, causing a migration of the convection towards the region of maximum heating. Whereas the lateral scale of the variations produced by the Webster (1983) model were essentially correct, they occurred at twice the frequency of the observed events and were formed near the coastal margin, rather than over the ocean.

Webster's (1983) model used to pose the theories was deficient in a number of aspects. Particularly, both the ground moisture content and the thermal inertia of the model were severely underestimated. At the same time, the sea surface temperatures produced by the model between the equator and the model's land-sea boundary were far too cool. Both the atmosphere and the ocean model were modified to include a better hydrological cycle and ocean structure. The convective events produced by the modified model possessed the observed frequency and were generated well south of the coastline.

The improved simulation of monsoon variability allowed the hydrological cycle feedback to be generalized. It was found that monsoon variability was constrained to lie within the bounds of a positive gradient of a *convective intensity potential (I)*. The function depends primarily on the surface temperature, the availability of moisture and the stability of the lower atmosphere which varies very slowly on the time scale of months. The oscillations of the monsoon perturb the mean convective intensity potential causing local enhancements of the gradient. These perturbations are caused by the hydrological feedbacks, discussed above, or by the modification of the air-sea fluxes caused by variations of the low level wind during convective events. The final result is the slow northward propagation of convection within an even slower convective regime. The ECMWF analyses show very similar behavior of the convective intensity potential. Although it is considered premature to use the model to conduct simulations of the African monsoon system, the ECMWF analysis indicates similar behavior in the convective intensity potential suggesting, at least, that the same processes control the low frequency structure of the African monsoon. The implications of the hypotheses on numerical weather prediction of monsoon phenomenon are discussed.

## 1. Introduction

There are probably three fundamental driving mechanisms of the planetary scale monsoon. The first mechanism is the differential heating between the land and the ocean and the resultant longitudinal anomaly in the zonally symmetric heating gradient of the annual cycle. The second is the impact of planetary rotation which produces

latitudinal character into the dynamic response of the atmosphere to the differential heating perturbations. The third mechanism relates to the critical role the hydrology cycle plays in the monsoon. Moist processes appear to determine the strength, vigor and location of the major monsoon precipitation by storing, redistributing and selectively releasing, in the vicinity of the heated continents, the solar energy absorbed over most of the tropical and the subtropical oceans (Webster, 1987). Moist processes also appear to be instrumental in producing low frequency variability on subseasonal time scales (Webster, 1983).

Another view of the monsoon, which seems quite consistent with the above, is that it may be considered to be a manifestation of the seasonal migration of the intertropical convergence zone (ITCZ) in the vicinity of the major continental regions. The intraseasonal variation of the summer monsoon rainfall over the continental regions is associated with the variation in location and intensity of the ITCZ and the degree of activity over a particular region.

### *1.1 The Observed Intraseasonal Variation of Monsoon Systems*

Studies elucidating the observed nature of the low-frequency variability of the monsoon have found principal energy peaks in the 10–20 and 30–50 day scales (e.g., Krishnamurti and Bhalme, 1976; Yasunari, 1979; Sikka and Gadgil, 1980; hereafter referred to as S&G). The detailed satellite imagery studies by S&G have shown that the ITCZ appears as the prominent cloud band in the monsoon system and have revealed a rich structure of supersynoptic[1] scale variation over the South Indian longitudes during the summer.

Figure 1 (S&G), shows examples of the variation of the ITCZ as a function of time along the 90° E, 80° E and 70° E meridians. The variation is manifested as a succession of events, occurring within a well defined seasonal envelope, which involve the genesis of the ITCZ over the South Indian Ocean near the equator, followed by an active

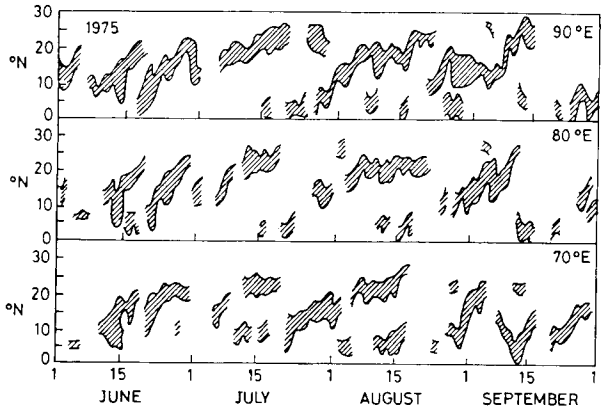


Fig. 1. The latitudinal locus of the maximum cloud zone obtained from satellite imagery at 70°, 80° and 90° E during the summer of 1975. Note the low frequency propagations from the equator to the north and the coherence that exists across the Indian Ocean from west to east. Dual maxima occasionally exist with convection occurring near the equator and well northward over South Asia. Mostly, the propagations are poleward with only occasional hints of a reversal. From S&G

spell (which may or may not involve a northward propagation in space) and a demise, or a decrease in intensity, usually in the north. Across South Asia, there appears to be considerable coherence. Figure 1 shows that the time and latitudinal structure is much the same across the entire Indian Ocean. Unfortunately, it is difficult to assess whether or not there is any longitudinal lag.

From the Sikka–Gadgil analysis, there appears to be two favorable locations for the ITCZ: one over the warm waters of the equatorial Indian Ocean and the other over the heated continent in the vicinity of the seasonal trough. Thus, the latitudinal distribution of the occurrence of the ITCZ appears to be bimodal with the zone of frequent occurrence over the continent and a secondary zone over the equatorial oceans. S&G suggest that there is a seesaw in the activity of the continental and oceanic ITCZ's with active spells of one coinciding with weak spells of the other. The most prominent feature of the intraseasonal variation is the poleward propagation of the oceanic ITCZ onto the continent between the geographic limits of the seesaw. The propagations begin in the onset phase of the monsoon and occur throughout the summer season.

The genesis of the ITCZ over the land and the ocean appears different. Over the continents, the

[1] The terms supersynoptic, subseasonal and intraseasonal are used interchangeably in various articles to explain weather events that are longer in time scale than weather events but are less than seasonal in duration.


ITCZ revives either by genesis of the ITCZ over the continent or by northward propagations from the ocean regions and across the continent. However, the revival of the oceanic ITCZ occurs only by genesis over the ocean. That is, while there are propagations from the ocean to the continents, the reverse propagation is rarely, if ever, observed. Thus, while there are clear propagations from the ocean to the continent, there are no low frequency propagations apparent from the land to the ocean. A major aim in this study is to understand the mechanisms underlying the unidirectional propagations of the maximum convective zone, or, alternatively, the ITCZ.

The interval between two successive propagations varies considerably within the season, and also from year to year. During the onset phase, the period is rather short but generally about 40 days once the monsoon is established. Note that the propagations have similar time scales to the Madden–Julian 40–60 day mode (Madden and Julian, 1971) but are displaced somewhat poleward. Hartmann and Gross (1988) have noted the northward displacement of the Madden–Julian mode during the boreal winter.

Compared to the Asian monsoon system, the African monsoon has received scant attention. In a sense, this is surprising as the African monsoon was the first monsoon system to be identified (Halley, 1686) and it affords the same societal significance as the Asian system. What work there is on the subject appears to describe the mean structure (e.g., Hendl, 1963; Walker, 1960) or specific phenomena within the monsoon system (e.g., Flohn, 1960; Ramage, 1971; Johnson, 1962). During the past few years, following considerable rainfall failures in northern Africa, there have been a number of observational (e.g., Nicholson, 1980, Hastenrath and Lamb, 1979, Hastenrath 1988, for review) and modeling studies (Palmer, 1986) that have attempted to relate precipitation extrema with other climatological variability such as the El Niño-Southern Oscillation (ENSO) cycle.

A study, in the spirit of S&G, has been undertaken by Gadgil and Asha (1988, 1991). Following the definition of an albedo-infrared algorithm for satellite data for the identification of deep convection, Gadgil and Asha extended the analyses of S&G to other parts of the globe. Along the 30° E meridian they found significant low frequency (multi-week) activity in the southern hemisphere during the austral summer. However, along 10° E during the boreal summer, they found low frequency variability to be less defined and subject to a greater interannual variability than occurred over South Asia.

### *1.2 Modeling the Intraseasonal Variations of the Monsoon*

Hahn and Manabe (1975) using the GFDL general circulation model, found an occurrence of two favorable locations over the same longitudinal belt with a seesaw in the activity of the two convergence zones. However, in their simulation, the revival of the continental ITCZ from weak spells occurs by genesis in the same latitudinal belt. No poleward propagations from the ocean into the continent were apparent, or, at least, obvious from their analyses. Goswami and Shukla (1984), using a symmetric version of the GLAS general circulation model, obtained similar results but with considerable evidence of propagation. With a zonally averaged axisymmetric climate model developed initially by Webster and Lau (1977), Webster and Chou (1980a, b) simulated the northward propagations of the ITCZ. The model geometry was spherical with a zonally symmetric continental cap placed north of 14° N[2]. The remainder of the globe was covered by an advective-mixed layer upper ocean model (Webster and Lau, 1977).

A comparison between observations and the results of the W-model reveals the strengths and weaknesses of earlier simulation attempts. Figure 2a shows a smoothed version of the ITCZ locus along 90° E (from Fig. 1) while Fig. 2b shows the locus of the maximum upward vertical velocity field during a typical year of integration of the original W-model (Webster, 1983). The intraseasonal variation comprises a succession of ITCZ events involving genesis at the land-ocean boundary and subsequent poleward propagation, similar, to some extent, with observations. Subsequent analyses and interpretation of the results were made by Webster (1983). However, the onset over the continent in the model is less complex than observed. The propagations are also more orderly

[2] Henceforth referred to as the W-model. The "geography" of the model is assumed to represent the land-sea distribution along the 90° E meridian. The model is discussed in some detail in Section 2 of this paper.

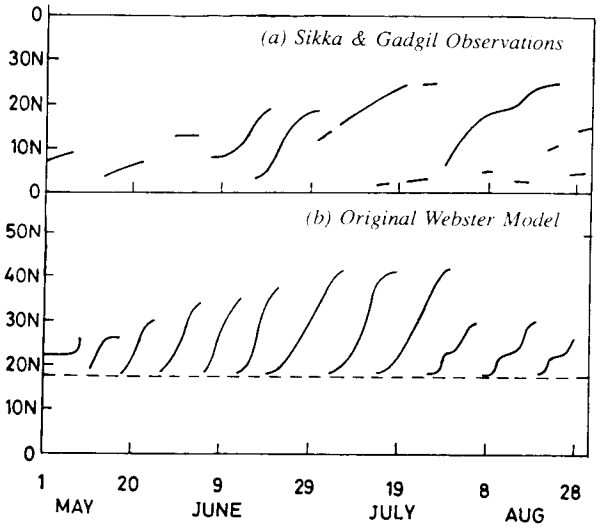


Fig. 2. The locus of the maximum vertical velocity as inferred from the satellite observations of S&G (upper panel) and from the original W-model (lower panel; Webster, 1983) during a typical year of integration. Note the rapid and more regular migrating events in the bottom panel compared to the lower frequency northward "drifts" in the lower panel

periodic propagations occurring at shorter intervals. The revival of the continental ITCZ occurs only through such poleward propagations. Also, while the observed propagations emanate from the equatorial ocean before propagating onto the land area (S&G), the W-model showed that the model ITCZ always formed at the land-ocean boundary so that the poleward propagations occur only over the land surface. Furthermore, the time scale of the propagations was considerably more rapid than in the real atmosphere. Also, the simulated sea surface temperature, especially between the land margin and the equator, is too cool.

### *1.3 Mechanisms of Propagation of the Intraseasonal Variations of the Monsoon*

Webster (1983) suggested that the poleward propagations of convective maxima arise in the model due to the north-south differential in total heating generated by surface hydrological feedbacks. The hypothesis suggests that the surface conditions at the lower boundary and the total heating in the atmospheric column are indelibly locked together through the hydrology cycle. Changes in the surface conditions, induced by precipitation in the atmosphere, cause changes in surface fluxes. These, in turn, alter the total heating gradient in the atmosphere causing the ITCZ to propagate poleward. The sense of the propagation was explained by noting that the impact of the hydrological feedback was to reduce the total heating equatorward of the ITCZ and to increase it poleward of the convection. The northward propagation is limited by the formation of a new ITCZ near the coastal margin which starves the more poleward system of moisture and reduces its total heating rapidly. According to Webster (1983), the lifetime of a single event, thus, is a function of the recovery time of the surface (i.e., the period required to dry the surface) in the high insolation region near the ocean. Alternatively, the regeneration of the convection is determined by the evaporative time scale of the land surface in the model.

Clearly, the observed propagations across the oceans cannot be understood strictly in terms of this feedback mechanism alone. However, similar feedbacks could occur with enhanced fluxes produced by the stronger winds within the disturbed band and the heating of the atmospheric column. But, as such oscillations over the ocean are not apparent in the W-model results (see Fig. 2b), then either the particular parameter range chosen for the model is incorrect or the physical processes used within the model are not properly handled.

### *1.4 Some Remaining Questions*

The intraseasonal variation of the South Asian monsoon provides the major weather variability in the monsoon regions during the established wet season. Whereas some progress has been made towards understanding the variability from a number of observational, theoretical and modeling studies, there are a number of remaining problems that require elucidation. These are:

(i) *The Time Scale of the Variability:* Model results indicate a far more rapid time scale of the interannual variability than that which is observed. What are the causes of the difference and what determines the observed time scale?

(ii) *The Region of Genesis of the Convective Zones*: Model results indicate that the genesis region of the convective events occurs at the ocean-continent boundary. Observations, on the other hand, suggest that genesis occurs much nearer to the equator than over the ocean. What is the reason for this discrepancy? What is the true formation mechanism for the convective events?

(iii) *The Propagation Mechanism:* Propagation occurs in some models but not in others. Webster (1983) suggests that the ground hydrological columnar heating feedback is responsible for the propagation polewards of the convective zone. Yet, propagation occurs in the real system over the ocean as well (S&G)! Is the mechanism proposed by Webster unique for the continental regions so that other propagation mechanisms are necessary over the oceans or is the ground hydrology mechanism applicable to the ocean as well? Is the failure a result of poor ocean modeling or limitations of the ocean-atmosphere flux parameterizations?

(iv) *Monsoon Forecasting:* The low-frequency intraseasonal variations of the monsoon correspond to the active and break periods of the monsoon which have crucial societal and economical significance. Is it possible to define the necessary requirements for a model or diagnostic scheme, based on the mechanisms resulting from successful explanations of (i) through (iii), above, to test the feasibility or to increase the skill in forecasting low frequency events? Also, the time scales of the phenomena in question fall between the short period and interannual periods. For the former scales, the forecasting problem is an initial value exercise relative to set boundary conditions. The latter period demands a fully interactive and dynamic coupled system. For the monthly to seasonal time scales there is uncertainty regarding the correct type of ocean to use in simulation and forecasting. For this reason, we include an interactive lower boundary which allows an evolving and deterministic sea surface temperature and ocean-atmosphere fluxes.

In this note, we report on the results of further detailed investigations of the low frequency variability of the monsoon using a derivative of the W-model. With some reasonable modifications of the model, new results indicate that the timescale of the propagations and their genesis regions are much more realistically simulated showing both a lower frequency and more equatorial formation region. These results are discussed in detail in Section 3. Experiments using a South Asian and an "oceanic" geography (the latter for comparison) are discussed. In Section 4, a generalized theory of propagation is provided. A comparison of simulated and observed results for all three cases with particular emphasis on the convective intensity potential, is given in Section 5 using ECMWF data. The results are summarized in Section 6 and their significance noted in relation to extended prediction and climate modeling.

## 2. The Monsoon Model

### 2.1 The Basic Model

There are two parts to the W-model: an ocean and a moist fully dynamic nonlinear atmosphere. The atmosphere and the ocean are coupled. The atmospheric model is totally prognostic driven only by an imposed annually varying solar heating function. The ocean model contains a mixed layer model which is in local equilibrium with the atmosphere and with the long and short wave radiative heating. Regional buoyancy imbalances are adjusted by advection. The former model is described in detail by Webster and Lau (1977) and the latter by Webster and Chou (1980a) and Webster (1983). Only pertinent elements of either model will be described here. A schematic diagram of the model is shown in Fig. 3.

In the design of the model we have made a very deliberate choice in using an interactive ocean model. A number of choices were available, of course, ranging from a constant sea surface temperature (SST) distribution to the assumption of a "perfect" ocean where an evolving SST, based

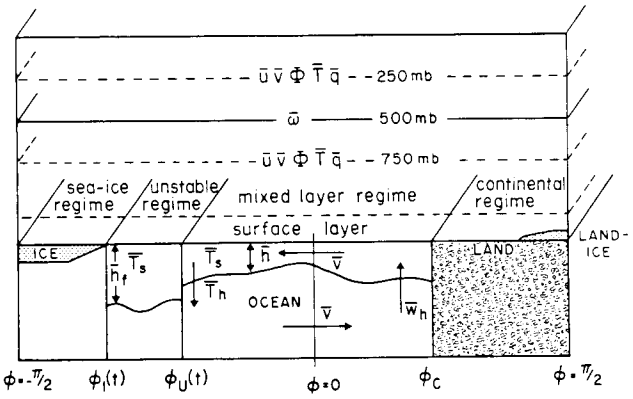


Fig. 3. Schematic diagram of the W-model (Webster and Chou, 1980a). The atmosphere is a two-layer moist primitive equation system placed over an interactive ocean and continental region. Radiation and interactive ground hydrology cycles are included in the model. The ocean is modeled by an advective mixed-layer model (Webster and Lau, 1976) which takes into account both gravitationally stable and unstable regimes and where buoyancy flux imbalances are corrected by advection. Time dependent land and sea ice models included

on climatology, would be provided. However, neither of the latter choices would provide a check on the accuracy of the interfacial fluxes produced by the model. As we will develop mechanisms that depend stringently on the magnitude and distribution of the surface fluxes, it was decided to use an interactive ocean, albeit a simple system.

In gravitationally stable regions, the advective mixed layer ocean model predicts the mixed layer temperature and depth. In gravitationally unstable regions, where a mixed layer becomes undefined, a convective adjustment scheme calculates the surface temperature. The transition points between the stable and unstable regions are calculated at each iteration. Horizontal density gradients produced by local imbalances drive a meridional heat transport. Sea-ice and land-ice formulations calculate time dependent ice limits. The temperature of the continental surface is calculated from energy balance considerations which take into account a full hydrology cycle, including precipitation.

The zonally symmetric formulation of the W-model is the nonlinear primitive equation system:

$$\frac{\partial u}{\partial t} + G(u) - v\left(f + \frac{1}{a}\tan\phi\right) = F_1 \tag{1}$$

$$\frac{\partial u}{\partial t} + G(v) + u\left(f + \frac{1}{a}\tan\phi\right) = -\frac{\partial \Phi}{\partial \phi} + F_2 \tag{2}$$

$$\frac{\partial T}{\partial t} + G(T) - \frac{kT\omega}{p} = Q_{tot} + F_3 \tag{3}$$

$$\frac{\partial \Phi}{\partial p} = -\frac{RT}{p} \tag{4}$$

$$\frac{\partial q}{\partial t} + G(q) = M + F_4 \tag{5}$$

and

$$\frac{\partial \omega}{\partial p} + \frac{\partial(v\cos\phi)}{a\cos\phi\,\partial\phi} = 0 \tag{6}$$

where $G$ is the nonlinear operator,

$$G(X) = -\frac{1}{a\cos\phi}\frac{\partial(Xv\cos\phi)}{\partial\phi} - \frac{\partial X\omega}{\partial p} \tag{7}$$

$T$, $q$, $u$, $v$ and $\omega$ represent the zonally averaged temperature, specific humidity, the zonal and meridional velocity components and the vertical velocity component, $dp/dt$, respectively. $Q_{tot}$ and $M$ represent the total heating rate of the atmospheric column and the moisture source and sink term. The $F_i$ represent the small scale dissipations of momentum, heat and moisture in (1), (2), (3) and (5), respectively.

The atmosphere is represented in the vertical by two layers at 250 and 750 mb. The zonal and meridional momentum and mass conservation equations are written at the 250 and 750 mb levels (model levels 2 and 1, respectively). The First Law of Thermodynamics is written at the interface of the two layers. Surface winds are assumed to be one half of the 750 mb vector winds.

### 2.2 *The Hydrology Cycle and Heating*

The total heating is given by:

$$Q_{tot} = Q_l + Q_s + Q_r \tag{8}$$

where $Q_l$, $Q_s$ and $Q_r$ are the latent, sensible and radiative heating rates of the column.

The latent heating of the column is comprised of two components: the heating due to broad scale convection ($Q_L$) and the convective heating in moist unstable regions ($Q_{CV}$) such that:

$$Q_l = Q_L + Q_{CV} \tag{9}$$

where

$$Q_L = \frac{L}{2C_p}(|q - q^*| + |q - q^*|) \tag{10}$$

and

$$Q_{CV} = \Delta\left[\int_0^{p_0} \left\langle \eta(1-b)\frac{L}{C_p}\overline{\omega q}\right\rangle dp\right]. \tag{11}$$

$q^*$ is a critical specific humidity at which it is assumed large scale convection commences. $\Delta$ is a Heaviside function given by:

$$\Delta = \begin{cases} 0, \omega \geqslant 0 \\ 1, \omega < 0 \end{cases}. \tag{12}$$

In essence, the convective parameterization expressed in (11) is a combination of the Ooyama (1969) and Anthes (1977) parameterizations introduced by Webster and Lau (1977). The degree of convection is determined by $\eta$, which controls the intensity of the convection, and by $b$, which governs the moisture availability. These controls are:

$$\eta = 1 + \frac{\theta_{eB} - \theta_{e_2}}{\theta_{e_2} - \theta_{e_1}} \tag{13}$$

and

$$b = \begin{cases} \dfrac{1-R}{1-R_c}, & R > R_c \\ 1, & R \leqslant R_c \end{cases} \tag{14}$$

$R$ is the relative humidity and $R_c$ is a critical value of $R$ set at 90%. Thus, $b$ increases linearly with $R_c$ from a minimum value of 1 at $R = R_c$. $\theta_{ei}$ is the equivalent potential temperature at level $i$ where $i = B$, 1 and 2. Level $B$ refers to the 990 mb level. For later reference, we define a convective intensity factor, $I$, as:

$$I = \eta(1-b)q_h. \tag{15}$$

The convective instability factor, $\eta$, is the ratio of the moist static instability of the lower troposphere (i.e., 1000–500 mb) to the moist static stability of the upper layer. $\eta$, thus, accounts for the enhancement of penetrative convection due to the conditional instability of the atmosphere. The moisture availability factor $(1-b)$ is a measure of the fraction of the moisture at the top of the boundary layer which is available for condensation. $\eta$, as well $(1-b)$, depends upon the surface temperature. $q_h$ is a measure of the boundary layer specific humidity in the two layer formulation. $I$ is, thus, a function of moisture availability and convective instability. From (13)–(15) it is clear that the convective latent heating depends upon other factors (e.g., the surface condition) as well as the vertical moisture flux.

In the original model, the surface temperature over land, $T_g$, was derived from an energy budget:

$$S_0 + F_d = \sigma T_g^4 + H_l + H_s \tag{16}$$

where $S_0$, the incoming solar radiation reaching the surface of the earth, is given by:

$$S_0 = (1-\alpha_n)\left(\frac{\pi}{2}\sin\phi\sin\delta + \cos\phi\cos\delta\right). \tag{17}$$

$F_d$ is the net longwave radiation at the surface. $\alpha_n$ is the albedo given by the formula:

$$\alpha_n = A_n + B_n \tanh C_n(T_n - T). \tag{18}$$

$H_s$ and $H_l$ are sensible and latent heat fluxes defined in (22) below. The subscript $n$, in (18), refers to the particular surface to which the albedo formulation is expressed. The values chosen for the model are listed in Table 1.

Table 1. *Albedo Law Constants*

| Constant | Land | Ocean |
|---|---|---|
| $A_n$ | 0.5 | 0.45 |
| $B_n$ | 0.3 | 0.35 |
| $C_n$ | 0.2 | 0.2 |
| $T_n$ | 270.0 | 268.0 |

We define a soil moisture content function, $W$. A critical value of $W$ (i.e., $W_c$) exists at which it is assumed that the ground has become saturated and that there will be run-off. When $W \geqslant W_c$, it is assumed that the surface albedo will decrease substantially to values similar to those over the ocean. Thus, the albedo over land may be written as:

$$\alpha_{land} = \begin{cases} 0.2 - 0.1\,W, & T > 273\,^\circ\text{K}, W < W_c \\ 0.1, & T > 273\,^\circ\text{K}, W \leqslant W_c \\ 0.8, & T \leqslant 273\,^\circ\text{K}, \end{cases} \tag{19}$$

The evaporation at the surface is given by:

$$E = \begin{cases} E_0, & W \geqslant W_c \\ E_0 \dfrac{W}{W_c}, & W < W_c \end{cases} \tag{20}$$

which, again, is highly dependent on the moisture content of the land surface, $W$, and the critical water holding capacity, $W_c$. Thus, when $W \geqslant W_c$, the evaporation is assumed to increase to oceanic values, (i.e., $E = E_0$), given similar surface temperatures (and, hence, saturated specific humidities) and other ambient conditions. The evaporation is calculated using the bulk formulation:

$$E_0 = \rho_s |V_s| C_d (q_s - q_h) \tag{21}$$

where the subscripts $s$ and $h$ refer to surface and 10 m values of the quantities, respectively. Equivalently, the sensible and latent heat fluxes are given by:

$$H_s = \rho_s C_D |V_s| C_p (T_s - T_h),$$

$$H_l = C_D |V_s| L(q_s - q_h) = \frac{C_D L}{C_p} E_0 \tag{22}$$

which provide the lower boundary inputs for the integrated columnar functions $Q_s$ and $Q_l$ defined in (8).

The moisture source and sink term, $M$ and the precipitation, $P$ are given:

$$M = C_p\left(\frac{1-b}{b}\right)\left(\frac{Q_l}{L}\right) \tag{23}$$

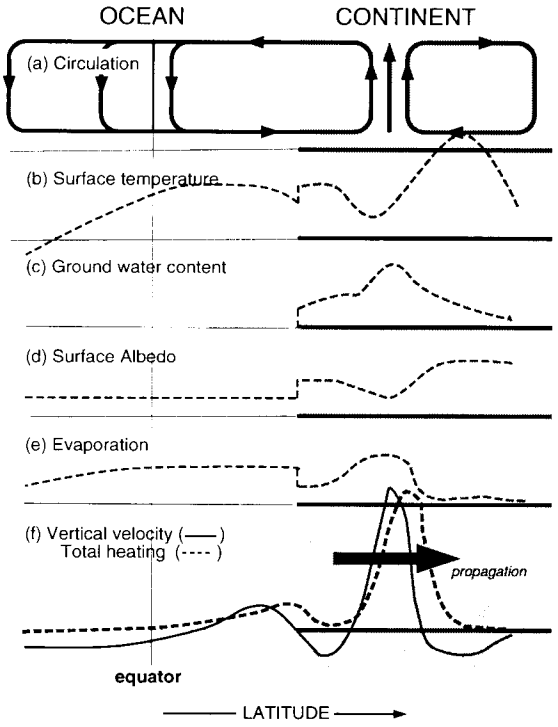


Fig. 4. Schematic diagram of the interactive hydrology cycle of the simple monsoon system modeled in this study indicating the degree of interaction between the atmospheric and surface hydrological processes. The figure shows the values of certain quantities as a function of latitude during the poleward propagation of a monsoon convective event (see Figs. 1, 2 and 9). The quantities are: (a) a typical monsoon circulation with maximum ascending motion over the continent, (b) the surface temperature (functional form given in Eq. (26)), (c) the ground water contained in the land surface (25), (d) the albedo (18 and 19), (e) the evaporation (20 and 21), and (f) the total heating (8) and vertical velocity in the atmospheric column

and

$$P = -\frac{1}{\rho_s g}\int_0^p M\,dp. \tag{24}$$

Final closure of the hydrology cycle is obtained by writing relationships between $W$, $P$ and $E$. Using the tendency of the ground water, we may write:

$$\frac{\partial W}{\partial t} = \begin{cases} 0, & W > W_c \\ P - E_0, & W < W_c \end{cases}. \tag{25}$$

Once again, the chosen value of $W_c$ is very important as it has the potential of feeding back directly into the surface albedo in (19) and the evaporation in (20). Through these two quantities, the entire surface energy budget in (16) and the total heating of the atmospheric column in (8) depends intimately on $W_c$. In other words, the ground hydrology pervades the entire model.

A more complete closure of the hydrology cycle would involve better handling of the radiation budget. The model could be improved in a number of ways. An interactive cloud scheme should be introduced so that clouds would become a deterministic quantity in the model. Also longwave emissivity of the atmosphere should be tied directly to the moisture content through (5). At the moment, cloud amount and emissivity are set as constant parameters. An optimal model would tie the cloud albedo and the emissivity together through one quantity which is a deterministic variable in the model such as through the liquid water path as proposed by Stephens (1978). The magnitude of the liquid water path can be obtained from the integrated water distribution from (6) although its distribution, most important for the longwave budget (see Stephens and Webster, 1981), is a more difficult problem.

Figure 4 provides a schematic representation of the coupling of the ocean and the continental land surface with the atmospheric circulation through hydrological processes. Over the ocean, the surface temperature is determined by the momentum transfer and turbulent mixing by the atmosphere and the insolation together with the heat budget at the ocean-atmosphere interface. Over land, the hydrological cycle impacts the surface albedo and evaporation. Coincident with the region of rising motion over the land area is the maximum precipitation and, thus, the maximum injection of ground water. Through (20) the evaporation is higher resulting in a local minimum in the surface temperature but a local maximum in latent heat flux. The local minimum in the temperature reduces the sensible heat flux so that the total impact of the hydrology cycle is to move $\omega$ and $Q_{tot}$ to be slightly out of phase with $Q_{tot}$ moved slightly towards the region of maximum temperature which is generally northwards. Note, too, that the increased precipitation lowers the local albedo through (19). As precipitation ceases as the convective event moves poleward, the local warming will be increased and evaporation enhanced.

Over the warm pool regions of the tropical oceans there is considerable precipitation, the ocean appears to be affected substantially by the fresh water flux into the ocean. The impact of the

flux is to stabilize the upper layer by the creation of a fresh lens. That is, precipitation creates a buoyant layer at the surface of the upper ocean. Erosion of this "barrier layer" (Lukas and Lindstrom, 1989) increases the mixing time scales of the ocean and increases substantially the temperatures of the upper layers. As the model utilized here does not contain explicit salinity as a free variable, the ocean cannot create a fresh lens. Thus, this process is absent from the model.[3] However, the surface fluxes used in the model are acutely sensitive to sea surface temperature as the saturation specific humidity in (21) and (22) is an exponential function of temperature through the Clausius–Clapeyron relationship. Thus, aspects of the warm pool interaction between the ocean and the atmosphere are included.

### 2.3 *Modifications to the Basic W-Model*

The differences between the W-model results and observations may result from model formulation deficiencies (e.g., an inadequate hydrological cycle). It is also possible that the model contains too few degrees of freedom and that the longer term variations in the real monsoon are driven by lateral dependencies, such as a globally propagating Madden–Julian wave (Madden and Julian, 1972) or longitudinal gradients such as suggested by Yang (1990). Neither effect could be simulated by a zonally averaged or symmetric model except through the crudest means. Nevertheless, we will make the assumption that the intraseasonal variability in the monsoon processes is influenced strongly by variations of the heating gradient along a meridian and that these processes are of zero-order significance. Furthermore, we will assume that a zonally symmetric model is an adequate model for the study of, at least, the basic phenomenology of the system.

We now modify the model in an attempt to remove deficiencies and to improve the simulations. It turns out that the deficiencies are relatively simple to address.

(i) *Surface Thermal Inertial:* Webster (1983) argued that the temporal variation of the model atmosphere is a response of the system to the variation of the conditions at the lower moist boundary, particularly over land. The response time of the land surface to variations in heating and dynamic interaction of the atmosphere depends on the thermal inertia of the boundary system. Since the response timescale of the land area is much smaller than that of the ocean, the thermal inertia of land is often taken to be zero as a first approximation in most climate models. This was the case in Webster's model. While this assumption has no serious consequences for the evolution of the monthly or seasonal fields, we could have anticipated that the impact of the underestimation of the thermal inertia on the intraseasonal variation be of greater significance. We have therefore, modified the W-model to incorporate a more reasonable thermal inertia of the ground. Hansen et al., (1983) suggested that an appropriate thermal capacity of the soil should be that which is commensurate with an equivalent depth of the annual thermal wave. This is assumed to be a depth of 4 m which is necessary in order to account for the seasonal heat storage in the soil. The thermal inertia of the surface system is incorporated in the following manner. (16) is adjusted to be a time dependent system such that:

$$C_E \frac{dT_g}{dt} = S_0 + I_d - \sigma T_g^4 - H_l - H_s \tag{26}$$

where $C_E$ is the effective volumetric heat capacity of the soil per unit area given by:

$$C_E = D_E C_v. \tag{27}$$

$D_E$ is the effective depth of the annual thermal wave which is assumed to be 4 m and $C_v$ as $1.125 \times 10^{-6}\,\mathrm{J\,m^{-3}\,K^{-1}}$ so that $C_E = 4.5 \times 10^6\,\mathrm{J\,m^{-2}\,K^{-1}}$ after Hansen et al. (1983). In effect, in the original Webster model, $C_E$ was set equal to zero which is tantamount to assuming instant equilibrium of the land surface energy balance to the imposed external fluxes.

(ii) *Critical Soil Moisture:* Webster (1983) assumed the maximum soil moisture holding capacity ($W_c$) to be 10 cm. We follow Hansen et al. (1983) using 30 cm as a more appropriate value for the Indian subcontinent. Consequently, the higher value was used in (25). Note that this adjustment will also have serious effects on the modification of time scales. (18) and (20), indicate that the increase in the critical soil moisture will take considerably longer to modify the albedo and evaporation.

[3] A discussion of the importance of the barrier is given in the International Science Plan of TOGA Coupled Ocean Atmosphere Response experiment (COARE) Webster and Lukas (1992).

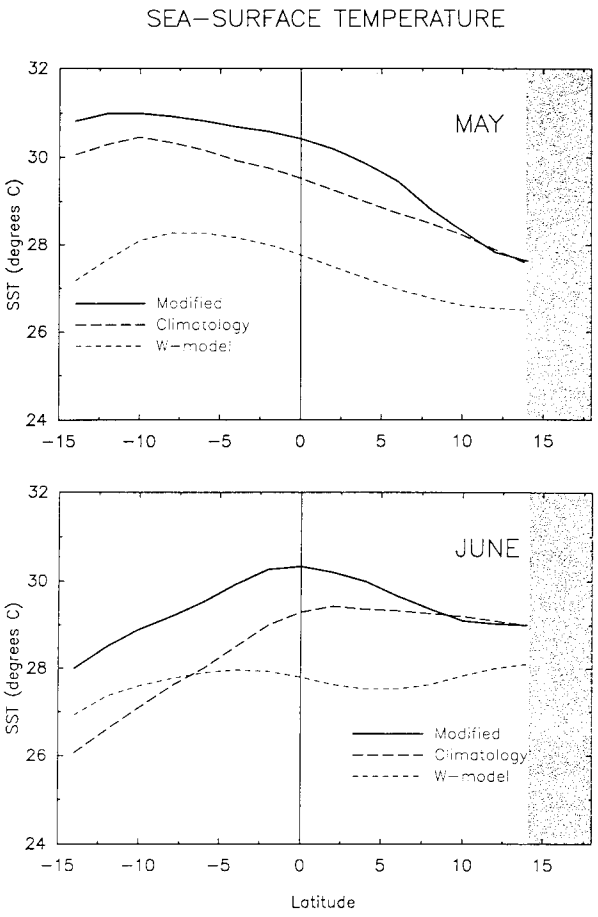


Fig. 5. The latitudinal distribution of the sea surface temperature (°C) calculated using the advective-mixed layer model in the original Webster model (thinner solid line) compared to the climatological values of Hastenrath and Lamb (1979) (dashed line) and the modified model developed in this study (heavier line)

(iii) *Sea Surface Temperature:* The sea surface temperature predicted by the Webster and Chou (1982a) and Webster (1983) coupled ocean-atmosphere model is somewhat lower than the summer climatological values over the South Asian longitudes. The underestimation resulted from the initial specification of too cool sub-thermocline between the equator and the coast. Following climatology, the sub-thermocline initial conditions were increased by 2.5 °C. Furthermore the upwelling mechanism in the model was apparently too strong and was reduced. A comparison of the climatological fields from Hastenrath and Lamb (1979), the adjusted model sea surface temperature fields and the calculated fields in the initial W-model (Webster and Chou, 1980a) are shown in Fig. 5. Although the SST's are now somewhat warmer than climatology, the SST minimum to the south of the continental area has been eliminated.

In summary, the modified version of the model contains three significant changes. The first two are related to the ground hydrology cycle of the model; the thermal lag of the ground was increased from zero to multi-day and the holding capacity of the ground increased by a factor of three, thus increasing the timescale of the response of the model surface. In addition, the initial conditions of the sub-thermocline sea temperature and sea surface temperatures were increased.

## 3. Simulation of the Variability of the Monsoon System

The model was integrated using the same geographic distribution as that used in the W-model. That is, a land sea boundary was set at 18° N as shown in the diagram at the bottom left of Fig. 6. Integration was continued for three years in order for the system to adjust to a cyclic equilibrium. Figure 6 the results for year 4 and depicts the latitude-time structure of the 750 and 250 mb zonal wind fields (panels a and b), the surface temperature (c), the vertical velocity (d) and the convective intensity potential (e). The model year (day 0) corresponds to the spring equinox. From the vertical velocity distribution, it is apparent that the model monsoon onset occurs at about day 30, indicating an in late April. During the early summer period, the surface temperature increases rapidly to the north of the coastline. Following the onset, all fields, including the surface temperature, are marked by distinct variability. With the onset, the first four major excursions of the vertical veloctiy occur. Each of these events are accompanied by rapid westerly accelerations at 750 mb and easterly acceleration at 250 mb. In fact, most of the events shown in Fig. 6 and those appearing in other years appear to have two distinct maximum, one to the north of the coast and the other well inland. In most cases, the vertical velocity maximum appears to propagate northward between the two extremes. Details of the vertical velocity distributions are shown in Fig. 7.

After the autumnal equinox (day 180), the variability of the monsoon decreases substantially. The model vertical velocity maximum decreases in magnitude and moves over the ocean and

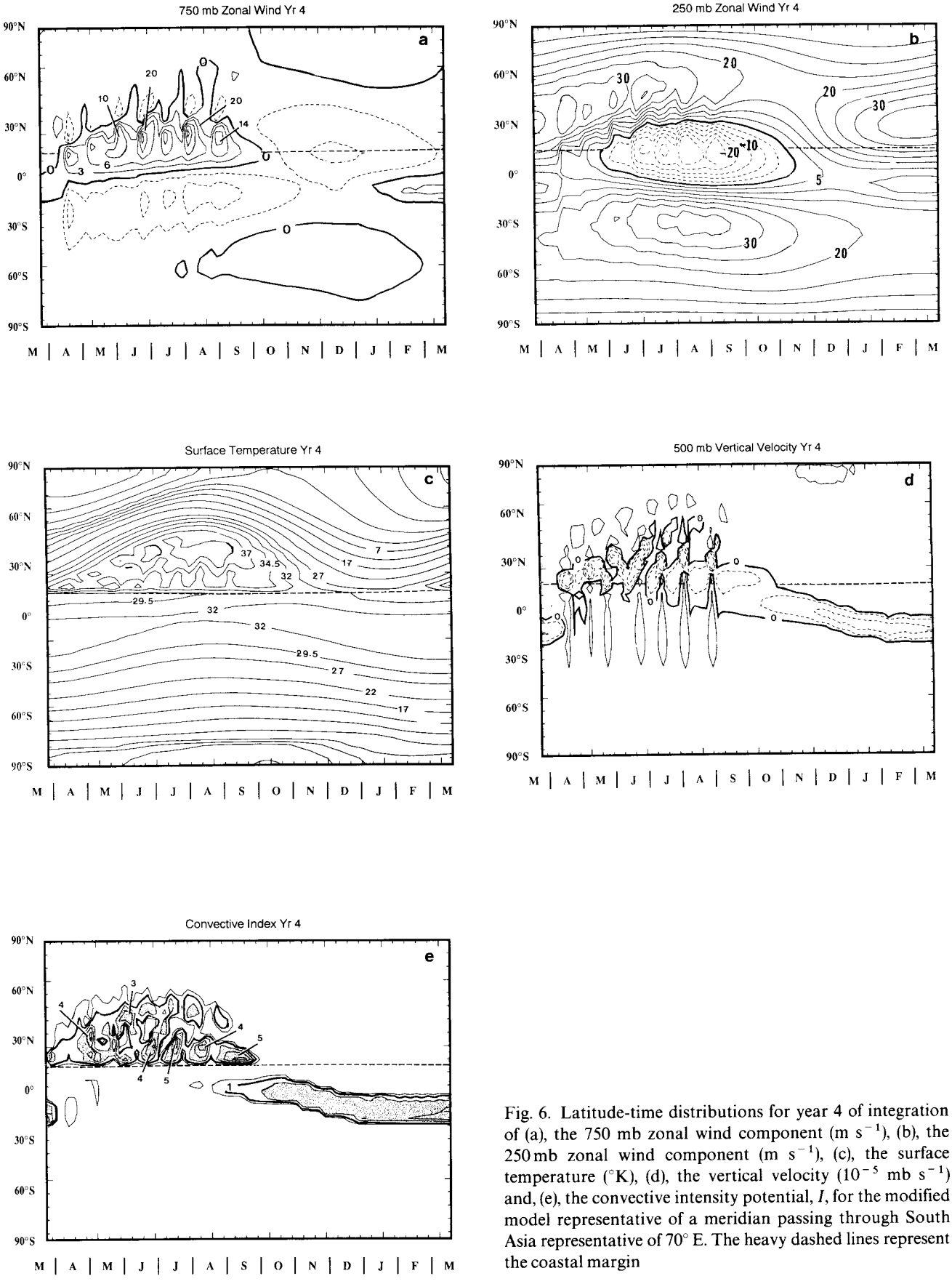


Fig. 6. Latitude-time distributions for year 4 of integration of (a), the 750 mb zonal wind component (m $s^{-1}$), (b), the 250 mb zonal wind component (m $s^{-1}$), (c), the surface temperature (°K), (d), the vertical velocity ($10^{-5}$ mb $s^{-1}$) and, (e), the convective intensity potential, $I$, for the modified model representative of a meridian passing through South Asia representative of 70° E. The heavy dashed lines represent the coastal margin

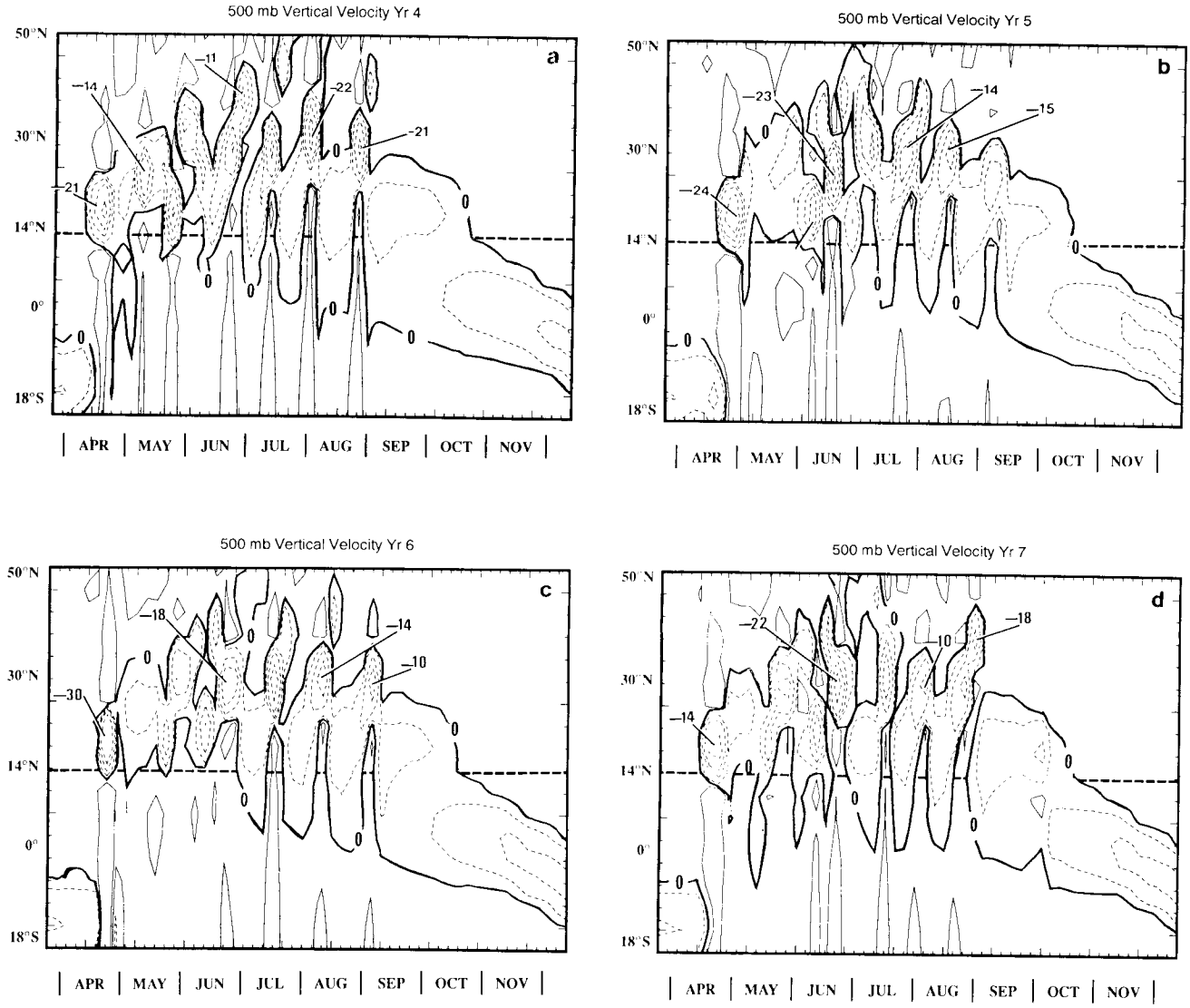


Fig. 7. Details of the vertical velocity distribution over the South Asian region of the summer months of years 4–7 of integration. (Units are $10^{-4}$ mb $s^{-1}$). Central values are indicated. Although each year tends to be different, the "events" tend to form in the south and move northward. In the early summer, the events tend to form over the continental regions and are associated with more erratic motion. Later in the summer the events form over the ocean region and move northward in a more regular fashion. In the autumn the migrations cease and the region of upward motion moves over the ocean as an "oceanic ITCZ"

follows the sea-surface temperature maximum where it remains until the next onset. During the boreal winter, the zonal velocity fields, very variable during the summer, also become slowly varying functions of time. In other words, monsoon variability seems to be constrained to the moist summer.

The convective intensity potential, $I$, (see panel e) shows a variation which is very similar to the surface temperature. Accompanying each of the poleward propagations, migration of the local $I$ maxima may also be seen. A very careful examination of Figs. 6a and e shows that a vertical velocity maximum appear to lie equatorward of the $I$ maximum. That is, the convective maxima appear to propagate only in regions of positive gradients of $I$. We will return to this point later.

Details of the vertical velocity distribution for years 4–7 are shown in Fig. 7. The latitude span is restricted to 20° S to 50° N and time from May to January. Whereas the general character of each of the years is similar (an onset in May followed by convective variability that slowly moves south-

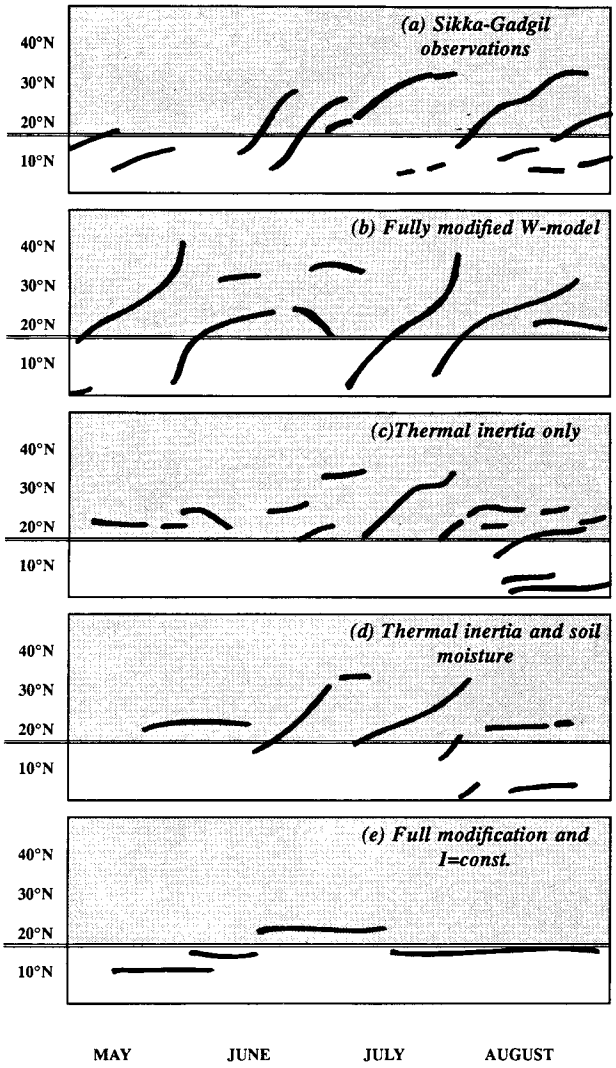


Fig. 8. Loci of the vertical velocity a function of time and latitude for (a), the 1975 observed fields, inferred from the analyses of the brightness data by S&G, (b), the fully modified model with an addition of thermal inertia term, an increase in the critical soil moisture value, $W_c$, from 10 to 30 cm, and the adjusted ocean model, (c), the modified model with only the thermal inertia change, (d), the modified model with the thermal inertia and critical soil moisture change, and, (f) the modified model with all changes but with the convective intensity potential, $I$, set equal to a constant value over the entire domain

ward over the ocean in the autumn) the details are very different with the number, phases and amplitudes of the events changing. For example, the number of events varies from only six in years 6 and 7 to eight in year 4. In general, the convective events commence over the ocean and move northwards over the land area. Occasionally, especially in early summer, the events appear to commence in situ over the continent and even propagate southwards. In autumn the convective events move over the ocean into the southern hemisphere.

Figure 8 provides a detailed breakdown of the impacts of the various modifications made to the original model. The upper two panels (labelled a and b) show, for reference, the locus of the Sikka-Gadgil cloud brightness and the original W-model vertical velocity as a function of latitude and time. Panel c shows the locus of the vertical velocity maxima from the modified model from Fig. 6d where all changes (i.e., increased thermal inertia and saturation ground water maximum and the adjusted initial ocean temperatures) are indicated. Comparing the modified model results and the observed fields, it is clear that, with the modifications, the frequency of the excursions and their genesis regions are now quite similar to the observational fields than before.

The incorporation of ground thermal inertia and the greater water holding capacity appears to have slowed down the role of heating of the continent and has delayed the onset of the monsoon until early May. Although this is still rather early compared to observations, it is a great improvement over the onset times of Webster and Chou (1980b) and Webster (1983). Note, too, that the convective events establish themselves well equatorward of the land-sea boundary marked as the horizontal double line.

The remaining panels of Fig. 7 show the impact of the individual model modifications. Panel d shows the effect of changing just the thermal inertia of the continental region of the model but still using the cooler sea surface temperature generated by the original Webster–Chou ocean model. Whereas the oscillations are now of a lower frequency, they are generally confined to the land area where the genesis regions are close to the land-sea boundary. Panel e shows the impact of including the more realistic critical soil moisture capacity of 30 cm. Now the excursions are considerably more northward probably because the ground near the coast takes much longer to dry out than in the original W-model. Also, the period of oscillation is now very similar to the observed time scale. Comparing panels e and c, it is obvious that the warmer sea surface temperatures produced by the adjusted ocean model allow the genesis of the events to occur over the ocean. In that sense, we may attribute the slower (and more realistic) time scales of the convective systems to the better modeled ground hydrology.

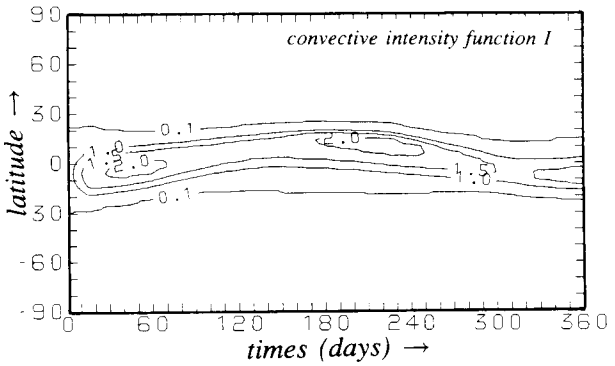


Fig. 9. Latitude-time distributions of the convective intensity potential, $I$, for the modified model representative of a meridian passing through the Pacific Ocean representative of the 180° meridian

At the same time, the more realistic locations of the genesis regions may be attributed to the warmer sea surface temperatures. Panel f shows the variability of the South Asian monsoon system when $I$ is set equal to a constant. The panel will be discussed in Section 4.

For later comparison with observations the model was configured to represent a mid-ocean geography. Figure 9 shows the convective intensity function for year 3 of the integration. Within the seasonal envelope, the fields are much smoother than their counterparts over the South Asian land mass shown in Fig. 6.

## 4. Mechanisms of Propagation

Webster (1983) noted that the proposed mechanism of propagation of the convective zones was generic in nature and that propagation would occur through any mechanism that would lead to the destabilization of the total heating-vertical velocity collocation. Over the continental regions, the destabilizing mechanism was produced by the interactive ground hydrology. Over the ocean, such mechanisms might be the variation of the surface fluxes resulting from changes in magnitude of the surface wind associated with the convection. In (22), we note that the latent and sensible heat fluxes, $H_l$ and $H_s$ depend linearly on the magnitude of the surface wind. Thus, it may be possible that if the sea surface temperatures were sufficiently warm, this second destabilizing mechanism may be of importance over the ocean. At the same time, we note that the latent heat flux is an exponential function of the SST through the saturation vapor pressure and the Clausius–Clapeyron equation.

### 4.1 Original Mechanism

Webster (1981) suggested that the ITCZ propagates northward from the point of genesis of the convective events (in this case near the land/ocean margin) due to larger total heating (i.e., the sum of convective and sensible heating) to the north of the ITCZ relative to the region directly beneath it or its south. That is, the convective maximum resides across a heating gradient and moves towards the region of greater heating. Webster (1983) suggested that the reduction of the sensible heat flux and the stabilization of the atmosphere over the wet land beneath and southwards of the ITCZ relative to the dry land in the north, plays a key role in generating the north-south differential in heating. According to the theory, the effects of ground hydrology is to make a collocation of $Q_{tot}$ and the vertical velocity impossible. This is because the vertical velocity, produced by a distribution of $Q_{tot}$, will immediately alter $Q_{tot}$ by producing precipitation which changes the ground hydrology and the surfaces fluxes. These, in turn, change the distribution of $Q_{tot}$. Thus, as long as the vertical velocity is associated with the ground hydrology (i.e., through precipitation), a steady state situation is not possible. The vertical velocity maximum,

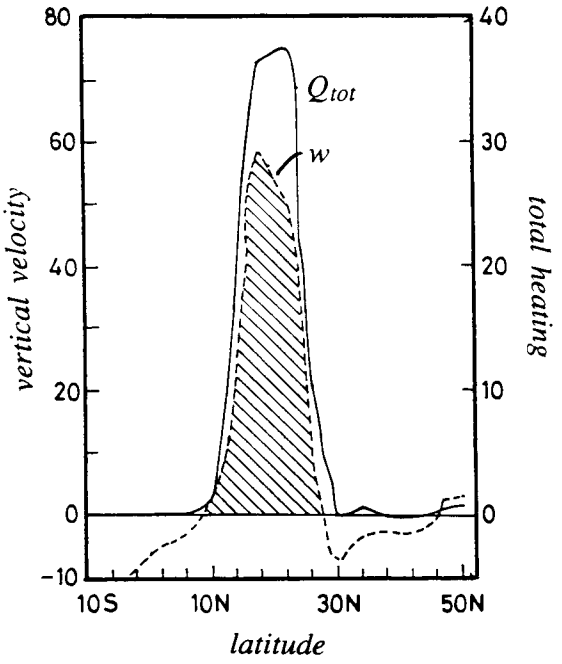


Fig. 10. The meridional profiles of the vertical velocity ($10^{-5}$mb s$^{-1}$, dashed line) and the total heating, $Q_{tot}$ (solid line) on a typical day during the northward propagation of an event

and hence the maximum convective zone, must migrate with a preferred direction of propagation towards the heating maximum.

Figure 10 shows the relative locations of the heating and the vertical velocity profiles at an arbitrary time during summer. As the region to the south of the convection is wetter than to the north due to previous precipitation, the total heating must increase northwards. Thus, the propagation increases poleward as long as the heating gradient has the same sign. A reversal of the heating gradient will occur when the southern limits of the land area, which lie in the higher insolation regions, dry out. At that stage, it was hypothesized, a new event developed, accompanying a reversal of the heating gradient in the north.

It is apparent that neither the observed propagations of the ITCZ (Fig. 1) nor those in the modified Webster model (Fig. 6) are restricted to land areas. Thus, a mechanism involving surface hydrological feedbacks, as described above, would seem to operate only on land and not in the ocean regime simply because the changes in the SST will evolve on time scales far slower than those of the convective events. Therefore, it is necessary to seek a more general mechanism for the propagation which can operate on land or the ocean.

### 4.2 Generalization

A key element in the extent of propagation of the convection appears to be the form and nature of the meridional variation of the convective heating (11), which is the dominant component of the heating function (8). The convective heating, $Q_{CV}$, in (11) is the product of the vertical moisture flux, and an intensity factor, $I$, defined in (15), which is a strong function of the surface temperature, which, in turn, is a strong function of the surface moisture. In the summer, the monthly or seasonal average values of each of these factors (and hence $I$) attain a maximum at the latitude of the maximum surface temperature, i.e., at the location of the mean seasonal trough induced by the solar insolation and the long term hydrological state of the land surface. Examples of the mean distribution of $I$ are given in Fig. 11 for the original W-model (dashed line) and the modified version (solid line). Both models show distributions of $I$ with maxima over the land areas near the location of maximum insolation. However, there are two main dif-

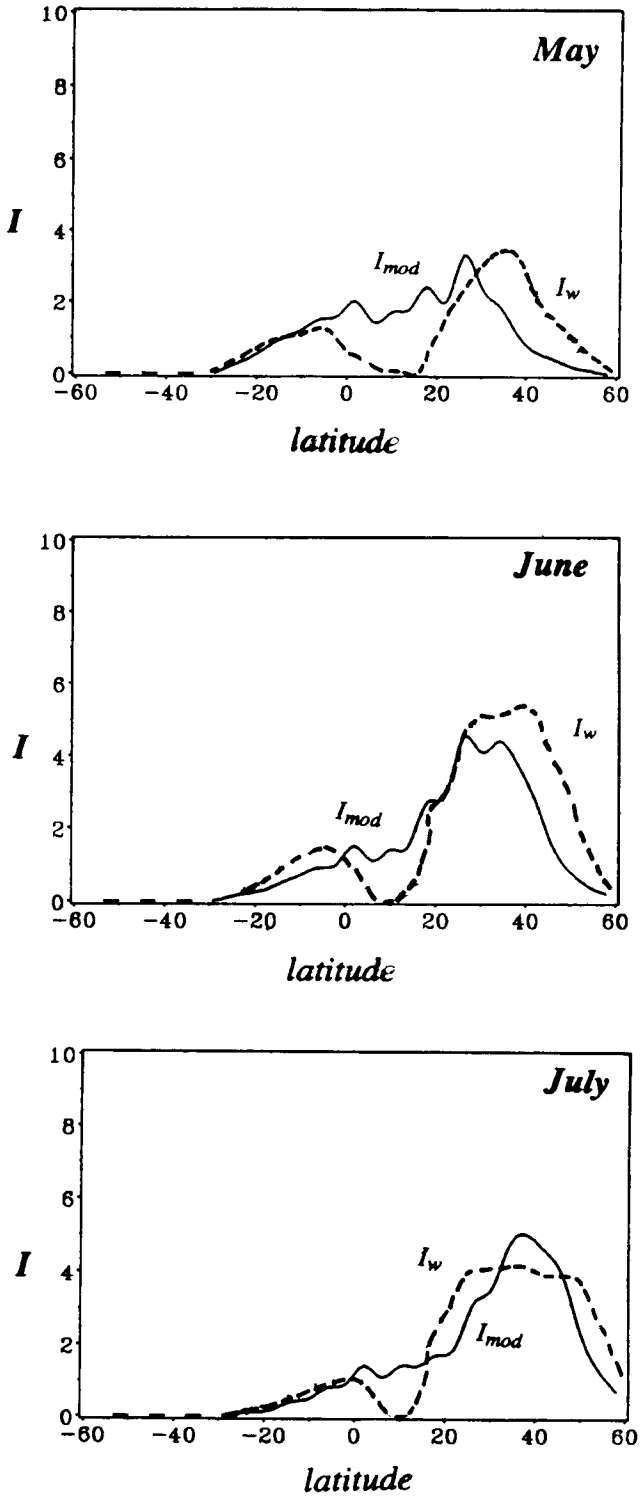


Fig. 11. Difference in the mean monthly value of the convective intensity potential, $I$ ($10^{-1}$), for the original W-model (dashed) and the modified model (solid) for May, June and July. Note, especially, the differences over the ocean and over the northern continental regions. In the modified model, the mean function possesses two maxima separated by a high valued saddle which spans the coast. In the original model, a zero exists at the coastline

ferences. The first is that the model modifications have produced much lower values than the initial model north of about 30° N, probably due to the layer thermal inertia term. The second, and the greatest, difference, is over the ocean. Here, the modifications have produced values of $I$ which are about an order of magnitude greater than were achieved in the earlier integrations. Over the ocean, $I$ appears to be extremely sensitive to sea surface temperature, probably because of the near saturation of the lowest layers of the atmosphere and the exponential increase of saturation vapor pressure with temperature.

In summary, with the simulation of a more realistic sea surface temperature, the mean $I$-profile has two maxima: one over the land regions and the other over the oceans. The second maximum coincides with the genesis region found in both the simulations (Fig. 6) and in observations (Fig. 1). Furthermore, the mean maximum over the land is larger than that over the ocean. Thus, in the mean there is a positive gradient of $I$ towards the north. That is, there exists, throughout the summer, the potential for a lag to exist between the vertical velocity profile and the total heating. Over land the lag is produced by the surface hydrology cycle. Over the ocean the lag is produced by the local enhancement of the ocean-atmosphere fluxes through the Clausius–Clapeyron effect and the local increases in low-level wind.

Examples of the variation of $I$ for the South Asian case as a function of latitude and time may be seen in Fig. 6e. The convection, and its subseasonal variations, determined from the vertical velocity distribution in Fig. 6b, is constrained to lie within a well defined positive envelope of positive values of $I$. Despite these subseasonal changes, the maximum value of $I$ persists in a similar location, corresponding to the location of the mean trough, in the daily profiles of $I$ throughout the summer. From (13) and (14), variations in the intensity factor $I$, may arise from various factors such as the changes in surface temperature due to hydrological feedbacks or changes in fluxes due to surface wind variations and the stabilization of the vertical enthalpy profile due to the mid-tropospheric heating associated with convection.

Figure 12 shows a sequence of the vertical velocity and $I$ sections through the model month of June. The shaded region shows the mean and monthly $I$-profile for June. An episode begins with

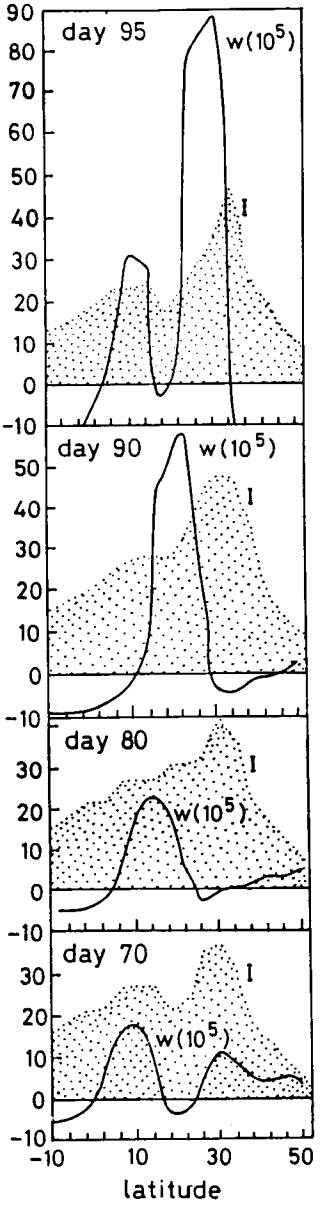


Fig. 12. Sequence of meridional profiles of the vertical velocity (solid line), the convective intensity potential, $I$ (dashed line) during the model month of June for the South Asia case (see Fig. 6) between days 70 and 95. The shaded area denotes the mean June–July distribution of $I$

a strong convective zone extending from 18–26° N (see Fig. 6d). Immediately following the demise of this event, a convective zone is generated over the ocean at about 6° N which slowly begins to propagate northward (Fig. 12a). The convective zone intensifies as it progresses poleward (Figs. 12b and c). As it reaches its maximum intensity (June 25, Fig. 12d), another mode forms over the ocean to continue the cycle.

The four sections (Figs. 12a–d) show considerable variability in the magnitude and the location of the vertical velocity. However, the deviations of the convective intensity potential from the monthly average are relatively small with the deviations reflecting the impact of the surface hydrology cycle. The most important point, though, is that the vertical velocity maximum is always to the south of the continental maximum of $I$. *That is, propagation of the subseasonal vertical velocity maxima is constrained to lie in the positive gradient of* $I$.

As the season progresses, the continental maximum of $I$ retreats with the insolation maxima and eventually disappears. The demise of the positive $I$ region over the continent can be seen in Fig. 6e. With this retreat, the northward limit of the propagations shrink southward until the maximum disappears. At this stage, the oceanic maximum predominates and the $I$-gradient reverses.

To test the control of the $I$ gradient in determining the character and location of the convection, the modified model was run with the intensity factor held constant over the entire domain. The impact of the constraint placed on $I$ was rather dramatic. The propagating character of the convection totally disappeared. Panel f of Fig. 7 shows the results of this experiment. Clearly, the ITCZ did not propagate. Thus, it may be concluded that the northward propagations depend primarily on the latitudinal variation of the intensity factor $I$ in the parameterization of convective heating in the model, which, in turn, arises from the seasonal insolation gradient, the background hydrological state of the continental surface and the sea surface temperature distribution.

In Figs. 6 and 7 it was noticed that in the early summer the convection commenced in situ over the continents rather than propagating from the ocean region. A careful examination of the fields indicates that the local maximum in $I$ which precedes the convective maximum is induced by a very strong sensible heat flux associated with the local maximum in surface temperature. As the sea surface temperature increases and the continental surface becomes wetter the area of large $I$ values increases and convection forms further to the south over the oceans.

The observed mean summer fields of the conditional instability and the specific humidity at the top of the boundary layer exhibit an increase with latitude in the summer hemisphere over the region equatorward of the latitude of the seasonal trough (Gray, 1968; Krishnamurti, 1979). Thus, the necessary condition for propagation of a positive meridional gradient of the intensity factor $I$, is likely to be satisfied by the tropical atmosphere in the region over which these propagations are observed. Hence, if the convective parameterization used in the model can be shown to be realistic, then the mechanism responsible for the observed propagations may have some credibility. We shall compare simulated and observed distributions of $I$ in the next section.

## 5. Observed Variations of the Convective Intensity Potential, $I$

Figure 13 shows latitude-time sections of the convective intensity potential during the summer of 1988 calculated from ECMWF data. The sections extend between the two poles along the 15° E, 75° E, 90° E, 120° E, and 180° E meridians. The African section was chosen for completeness. The 75° E, 90° E and 120° E sections represent the South Asian region (e.g., Figs. 6 and 7) and 180° E an ocean section (e.g., Fig. 9). The intensity potential was calculated from the ECMWF data in an identical manner to the calculation of $I$ in the model. The lower left panel shows the location of the meridians used in the calculation.

All five cases show an annual cycle but each with its own character. The Asian cases (i.e., 75° E, 90° E and 120° E) show a rather abrupt change in the locus of maximum variability some 30 days after the spring equinox (marked by the arrow on the abscissa). The ocean case (panel e) does not appear to possess any abrupt changes. The African case, on the other hand has a smaller range about the equator than the other three cases. Although the locus of maximum $I$ moves north of the equator during the northern summer, the axis of maximum convection remains close to the equator.

In the 75° E example, maximum subseasonal variability occurs during the northern summer in a manner similar to the South Asian case shown in Fig. 6. When the convection resides over South Asia, there are four periods of maximum $I$ with values of 5, 4, 5 and 4 units. This compares with four maxima of values 3, 5, 5 and 5 produced by

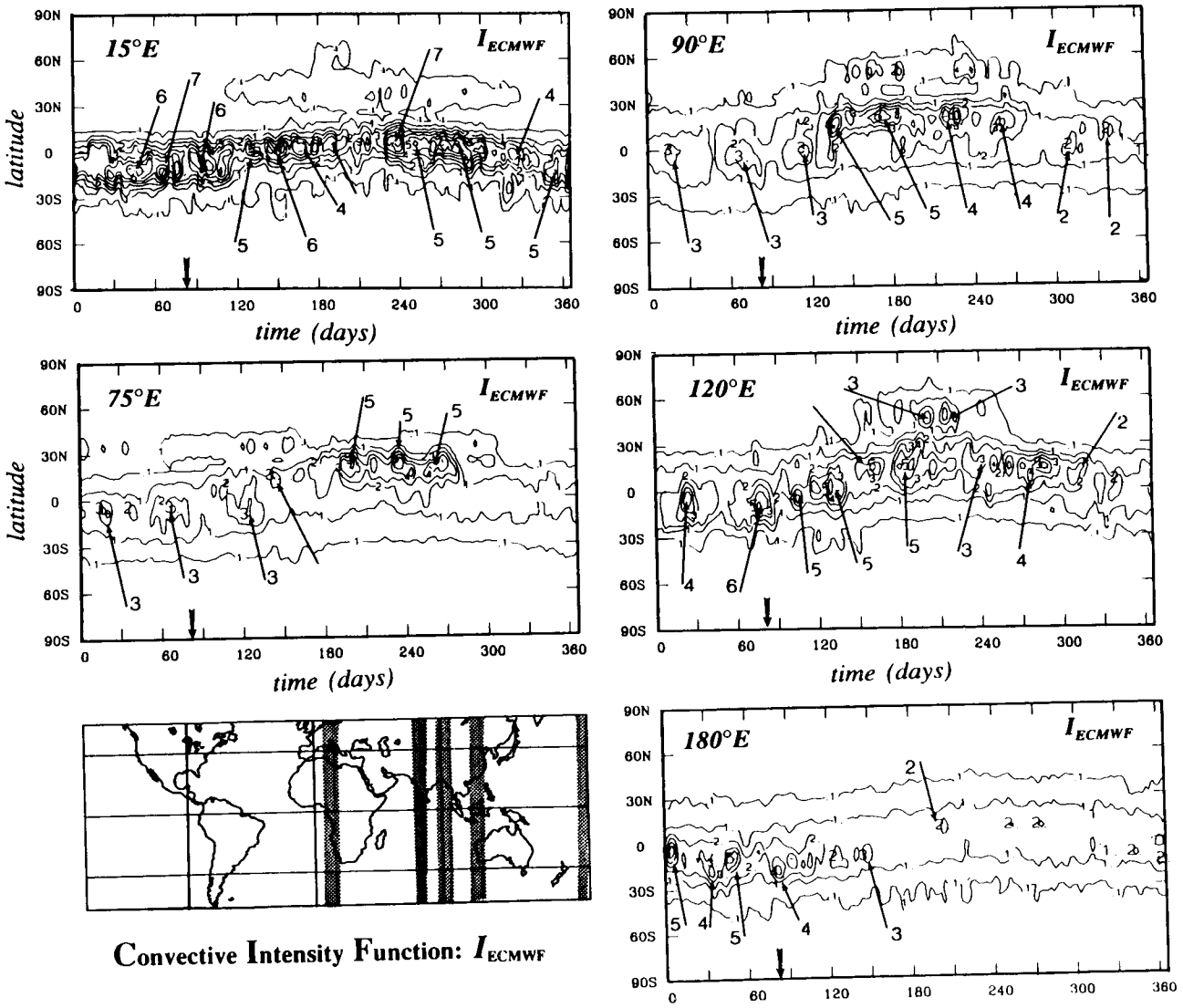


Fig. 13. Latitude-time sections of the convective intensity potential ($I$) calculated from ECMWF data during the summer of 1988 between 40° N and 40° S along (a) 15° E, (b) 75° E, (c) 90° E, (d) 120° E, and, (e) 180° E. The local maxima in $I$ ($10^{-2}$) are located by arrows. The meridians of the panels are shown as the shaded areas on the map

the model simulations. The observed variability of convection at other times of the year is relatively small, corresponding to times when the convection is over the equatorial and southern Indian Ocean. Thus, there is substantial agreement between the ECMWF realizations of convection and that produced by the model.

The 120° E section shows a similar annual variation to the 75° E and 90° E cases. However, the intraseasonal variability is quite different. Variation occurs throughout the year with about ten with values ranging from 2 to 6. Fairly strong coherence exists across the Indian Ocean which can be seen by noting the similar times the $I$ maxima occur at all three longitudes. S&G had found similar coherence in their satellite data across a similar longitudinal span. The extensive variability during the austral summer probably is associated with the Australian monsoon. Distinct convective episodes also exist over Africa with similar frequency and values to those found over Asia.

## 6. Summary and Conclusions

It has been shown that the incorporation of a more reasonable ground thermal capacity and critical ground water capacity and better oceanic

conditions in the Webster model produce better simulations of the transient behavior of the ITCZ in the vicinity of the Asian continent. Propagations of the convective maxima, as described above, depend on the existence of the seasonal distribution of $I$. The distribution of the intensity potential is set up by the impact of insolation on the continental regions and the sea surface temperature maxima near the equator. Clearly, the gradient of $I$ is a combined effect of ocean and continental impacts. Over the land areas, the meridional gradient of the sensible heat flux is also positive over the region, at least during the summer period and will tend to enhance, to some extent, the north-south asymmetry in the heating and thus, reinforce the propagations. Modulations of the land surface temperature by hydrological feedbacks and variations in the stability of the atmosphere will also have an impact on the detailed structure of the propagations.

Over other regions of the tropics where there does not exist a land mass poleward of the equator or an equatorial ocean (both of which are needed to produce a double maximum in the intensity potential), we would not expect there to be poleward propagations. In these cases, the $I$ function would have only one maximum coinciding with the sea surface temperature maximum. For the same reason, poleward propagations should not be expected (nor are they observed) during the winter monsoon over South Asia. McBride (1983), for example, finds little evidence of poleward propagations over the Australian continent during the Australian summer monsoon. Probably, this is due to the existence of only one maximum in $I$ over the north of Australia. That is, the northern coastline of Australia is too close to the equator to allow for the setting up of a second maximum in the intensity potential. Thus, the South Asian region is geographically unique in that it is sufficiently far away from the equator to be well poleward of the $I$ maximum produced by the sea surface temperature but sufficiently equatorward to possess an $I$ maximum produced by insolation.

Finally, it appears possible to learn something from the experiments and theories, described and expressed in this study, that will aid in extended weather and climate prediction. There are three major points that can be made which might ensure a better representation and prediction of the monsoon system. These are:

(i) *Sea surface temperature sensitivity:* The experiments indicated that there was considerable sensitivity to the surface temperature distribution. Clearly, in the simulation or extended prediction of the monsoon structure, care must be taken to use an accurate and interactive representation of the lower boundary. For climate forecasting purposes, the sensitivity of the forecast or simulation to the ocean temperature places an exacting role on the ability of the ocean model to predict properly the evolving sea surface temperature structure in simulations of the coupled system.

(ii) *Modeling the convective intensity potential, I:* The similarity of the magnitude and frequency of the observations and simulations of the convective intensity potential indicates that $I$ is a significant quantity. Thus, it is important that both the mean structure and variability be modeled with some accuracy. Modeling $I$ correctly requires careful attention to the convective scheme and to the surface processes at both the continental and oceanic interfaces that determine the value of $I$.

(iii) *Modeling the surface temperature gradient in moist environments:* As emphasized previously, the convective intensity potential is very sensitive relative to the surface temperature. Indeed, the sea surface temperature maximum near the equator and the surface temperature maximum provide the two $I$ maxima between which the convective maxima oscillate. Thus, to provide the slowly varying envelope of the latitudinal variation of convection, the annual cycle must be modeled carefully. In order to model the higher frequency variations of $I$, which appear to determine the sub-structure of the convection, it is necessary to model properly the interaction of the ground hydrology and the columnar heating to incorporate the feedback mechanism of Webster (1983) over the land areas.

The discussion above relates only to the physical processes which are local to the longitudes of South Asia and, perhaps, to the African region. It does not take into account the relationship of those longitudes with other regions nor the propagation into the region of other low frequency weather events such as the Madden–Julian mode (Madden and Julian, 1972). Hartmann and Gross (1988) have indicated that the summer precipitation patterns are affected by these modes although it has yet to be determined what the role of the monsoon regions is, if any, in the genesis or

modification of these modes. At the same time, the study has not addressed the importance of orography in the monsoon systems, especially the Himalayas in the South Asian monsoon. How the orography interacts and modifies the distributions of the mean and transient intensity potential must be subject of another study. In any event, an accurate modeling or prediction of the monsoon variability is a global problem. We point out only those processes which must be handled with special care in the monsoon regions themselves.

**Acknowledgements**

This work was undertaken under the auspices of the Indo-US Science and Technology Initiative on Monsoons. Support for the research was provided by the Atmospheric Science Division of the National Science Foundation under the grant ATM-9214840. We would like to thank Dr. Song Yang for considerable input.

**References**

Anthes, A. R., 1977: A cumulus parameterization scheme utilizing a one-dimensional cloud model. *Mon. Wea. Rev.*, **105**, 270–286.

COARE: The TOGA Coupled Ocean Atmosphere Response Experiment, TOGA COARE Science Plan, WMO Publication, Addendum No. 3.

Flohn, H., 1960: Equatorial westerlies over Africa, their extension and significance. In: Bargman, D. J. (ed.) *Tropical Meteorology in Africa.* Nairobi: Munitalp Foundation, 253–267.

Gadgil S., Asha, G., 1988: Poleward propagations of the intertropical convergence zone. Rev. 88 AS 2, Centre for Atmospheric Sciences, Indian Institute of Science, Bangalore, India.

Gadgil, S., Asha, G., 1991: On poleward propagations of the intertropical convergence zone. *Mon. Wea. Rev.* (submitted).

Gray, W. M., 1968: Global view of the origin of tropical disturbances and storms. *Mon. Wea. Rev.*, **96**, 669–700.

Goswami, B. N., Shukla, J., 1984: Quasi-periodic oscillations in a zonally symmetric general circulation model. *J. Atmos. Sci.*, **41**, 20–37.

Hahn, D. G., Manabe, S., 1975: The role of mountains in the South Asian monsoon. *J. Atmos. Sci.*, **32**, 1515–1541.

Halley, E., 1686: An historical account of the trade winds and the monsoons, observable between and near the tropics, with an attempt to assign the physical cause of the said winds. *Phil. Trans. Roy. Soc. London*, **16**, 153–168.

Hansen, J., Russell, G., Rind, D., Stone, P., Lacis, A., Lebedeff, S., Ruedy, R., Travis, L., 1983: Efficient 3-dimensional global models for climate studies: Models I and II. *Mon. Wea. Rev.*, **111**, 609–662.

Hartmann, D. L., Gross, J. R., 1988: Seasonal variability of the 40–50 day oscillation in wind and rainfall in the tropics. *J. Atmos. Sci.*, **45**, 2680–2702.

Hastenrath, S., Lamb, P., 1979: *Climatic Atlas of Indian Ocean Part I.* Madison: The University Wisconsin Press.

Hastenrath, S., 1988: *Climate and Circulation of the Tropics.* Dordecht: Atmospheric Sciences Library, D. Radel Publishing, Co., 455 pp.

Hendl, M., 1963: *Systematische Klimatologie.* Berlin: Veb Deutscher Verlag der Wissenschaften.

Johnson, D. H., 1962: Rain in East Africa. *Quart. J. Roy. Meteor. Soc.*, **88**, 1–19.

Krishnamurti, T. N., 1979: *Compendium of Meteorology*, Vol. II, Part 4. Geneva, Switzerland: World Meteorological Organization.

Krishnamurti, T. N., Bhalme, H. H., 1976: Oscillations of a monsoon system. Part I: Observational aspects. *J. Atmos. Sci.*, **33**, 1937–54.

Lukas, R., Lindstrom, E., 1987: The mixed layer of the western Pacific Ocean. In: Muller, P., Henderson, D. (eds.) *Proceedings of the "Aha Huliko'a 'Hawaiian Winter Workshop on the Dynamics of the Oceanic Surface Mixed Layer".* Honolulu, Hawaii, Hawaii Institute of Geophysics Special Institute Pub., pp. 69–74.

Madden, R. D., Julian, P., 1971: Detection of a 40–50 day oscillation in the zonal wind in the tropical Pacific. *J. Atmos. Sci.*, **28**, 702–708.

McBride, J. L., 1983: Satellite observations of the southern hemisphere monsoon during Winter MONEX. *Tellus*, **35A**, 189–197.

Nicholson, S. E., 1980: The nature of rainfall fluctuations in subtropical West Africa. *Mon. Wea. Rev.*, **108**, 473–487.

Ooyama, K., 1969: Numerical simulation of the life cycle of tropical cyclones. *J. Atmos. Sci.*, **26**, 3–40.

Palmer, T. N., 1986: Influence of the Atlantic, Pacific and Indian Oceans on Sahel rainfall. *Nature*, **322**, 251–253.

Ramage, C. S., 1971: *Monsoon Meteorology.* (International Geophysics Series, **15**) New York: Academic Press, 296 pp.

Sikka, D. R., Gadgil, S., 1980: On the maximum cloud zone and the ITCZ over Indian longitudes during the Southwest monsoon. *Mon. Wea. Rev.*, **108**, 1840–1853.

Stephens, G. L., 1978: Radiative properties of extended water clouds, Part I. *J. Atmos. Sci.*, **35**, 2111–2122.

Stephens, G. L., Webster, P. J., 1981: Clouds and climate: Sensitivity of simple systems. *J. Atmos. Sci.*, **38**, 235–247.

Walker, H. O., 1960: The monsoon in West Africa. In: Basu, S. et al. (eds.) *Monsoons of the World.* New Delhi: Hind Press, pp. 35–42.

Webster, P. J., 1983: Mechanism of monsoon low frequency variability: Surface hydrological effects. *J. Atmos. Sci.*, **40**, 2110–2124.

Webster, P. J., 1987: The variable and interactive monsoon. In: Fein, J. S., Stephens, P. L. (eds.) *Monsoons.* New York: John Wiley and Sons, 269–330.

Webster, P. J., Lau, K. M. W., 1977: A simple ocean-atmosphere climate model: Basic model and a simple experiment. *J. Atmos. Sci.*, **34**, 1063–1084.

Webster, P. J., Chou, L., 1980a: Seasonal structure of a simple monsoon structure. *J. Atmos. Sci.*, **37**, 354–367.

Webster, P. J., Chou, L., 1980b: Low frequency transitions of a simple monsoon system. *J. Atmos. Sci.*, **37**, 368–382.

Webster, P. J., Lukas, R., 1992: TOGA COARE: The Coupled Ocean – Atmosphere Response Experiment. *Bull. Amer. Meteor. Soc.*, **73**, 1377–1416.

Yang, S., 1990: Atmospheric teleconnections: Emphasis on

El Niño/Southern Oscillation and Monsoons, Ph.D. Thesis, The Pennsylvania State University, 228 pp.

Yasunari, T., 1979: Cloudiness fluctuations associated with the northern hemisphere summer monsoon. *J. Met. Soc. Japan*, **57**, 227–242.

Authors' addresses: J. Srinivasan and S. Gadgil, Centre for Theoretical Studies, Indian Institute of Science, Bangalore, India; P. J. Webster, Program in Atmospheric and Oceanic Sciences, University of Colorado, Campus P.O. Box 391, Boulder, Colorado, 80309-0391, U.S.A.